Nano Energy 112 (2023) 108460

Contents lists available at ScienceDirect

Nano Energy

journal homepage: www.elsevier.com/locate/nanoen

Face mask integrated with flexible and wearable manganite oxide respiration sensor

Lianxu Ye [a], Fan Wu [b], Ruixing Xu [c], Di Zhang [d], Juanjuan Lu [d], Chuanlong Wang [e], Anjiang Dong [e], Sichen Xu [e], Lejun Xue [e], Zixin Fan [f], Longjie Xu [a], Kaifeng Li [a], Dong Li [a], Ahmed Kursumovic [g], Run Zhao [f], Rujun Tang [e], Lei Qiu [i], Haiyan Wang [d], Judith L. MacManus-Driscoll [g], Qingshen Jing [h,*], Weiwei Li [a,i,**], Hao Yang [a,i,**]

[a] College of Physics, MIIT Key Laboratory of Aerospace Information Materials and Physics, Nanjing University of Aeronautics and Astronautics, Nanjing 211106, China
[b] College of Automation Engineering, Nanjing University of Aeronautics and Astronautics, Nanjing 211106, China
[c] School of Microelectronics & Data Science, Anhui University of Technology, Maanshan 243002, China
[d] School of Materials Engineering and School of Electrical and Computer Engineering, Purdue University, West Lafayette, IN 47907, USA
[e] Jiangsu Key Laboratory of Thin Films, School of Physical Science and Technology, Soochow University, Suzhou 215006, China
[f] Jiangsu Key Laboratory of Micro and Nano Heat Fluid Flow Technology and Energy Application, School of Physical Science and Technology, Suzhou University of Science and Technology, Suzhou 215009, China
[g] Department of Materials Science & Metallurgy, University of Cambridge, 27 Charles Babbage Road, Cambridge CB3 0FS, UK
[h] James Watt School of Engineering, University of Glasgow, Glasgow, UK, G12 8LT
[i] State Key Laboratory of Mechanics and Control for Aerospace Structures, Nanjing University of Aeronautics and Astronautics, No. 29 Yudao Street, Nanjing 210016, China

ARTICLE INFO

Keywords:
Sensor
Flexible electronic devices
Functional oxide films
$La_{1-x}Sr_xMnO_3$
Mica

ABSTRACT

Face masks are key personal protective equipment for reducing exposure to viruses and other environmental hazards such as air pollution. Integrating flexible and wearable sensors into face masks can provide valuable insights into personal and public health. The advantages that a breath-monitoring face mask requires, including multi-functional sensing ability and continuous, long-term dynamic breathing process monitoring, have been underdeveloped to date. Here, we design an effective human breath monitoring face mask based on a flexible $La_{0.7}Sr_{0.3}MnO_3$ (LSMO)/Mica respiration sensor. The sensor's capabilities and systematic measurements are investigated under two application scenes, namely clinical monitoring mode and daily monitoring mode, to monitor, recognise, and analyse different human breath status, *i.e.*, cough, normal breath, and deep breath. This sensing system exhibits super-stability and multi-modal capabilities in continuous and long-time monitoring of the human breath. We determine that during monitoring human breath, thermal diffusion in LSMO is responsible for the change of resistance in flexible LSMO/Mica sensor. Both simulated and experimental results demonstrate good discernibility of the flexible LSMO/Mica sensor operating at different breath status. Our work opens a route for the design of novel flexible and wearable electronic devices.

1. Introduction

Human health and lives are under threat by respiratory viruses (*e.g.* COVID-19) and other pathogens. Respiratory viruses can attack the human respiratory system such as lungs, leading to shortness of breath, lung damage, and impaired respiratory function [1–3]. The lungs are essential organs of the human body, when health conditions can be directly revealed by breath status [4,5]. However, abnormal breath parameters are frequently overlooked in many scenarios due to lack of proper monitoring equipment, which could indicate certain potential diseases [6]. For instance, breath rate is a valuable metric for determining clinical deterioration. A rising breath rate value beyond 27 min^{-1} is a predictive sign of cardiopulmonary arrest [7]. The abnormalities of breath, including imperceptible respiratory rate variability

* Corresponding author.
** Corresponding authors at: College of Physics, MIIT Key Laboratory of Aerospace Information Materials and Physics, Nanjing University of Aeronautics and Astronautics, Nanjing 211106, China
E-mail addresses: qingshen.jing@glasgow.ac.uk (Q. Jing), wl337@nuaa.edu.cn (W. Li), yanghao@nuaa.edu.cn (H. Yang).

https://doi.org/10.1016/j.nanoen.2023.108460
Received 9 March 2023; Received in revised form 11 April 2023; Accepted 17 April 2023
Available online 18 April 2023

(RRV) [8,9], and sudden shortness of breath [10], indicate a life-threatening alteration of the physiological status. A continuous, long-term, multi-modal breath monitoring strategy is highly demanded in clinical diagnosis and daily prevention.

Typically, breath rate of patients estimated by manual counting gives discrete values, which cannot provide continuous, detailed information about human respiratory status over a longer period of time or under changing conditions without subjectivity and variance [11]. Furthermore, traditional nosocomial breath monitoring technologies have significant drawbacks in accessibility for ordinary people due to their bulky size, high cost, and the requirement for professional operation. Given the remaining influence of the COVID-19 viruses, and other emerging infective pathogens are still affecting the world, it is highly demanded that respiration-related abnormality can be detected as earlier as possible for timely treatment. Meanwhile, wearing a mask is an effective approach to minimise the spread of viruses and prevent cross-infection [12]. Therefore, a breath monitoring module that utilizes the face mask as a carrier presents simplicity in collecting human breath parameters. The technological feasibility of monitoring human breath using a face mask based on piezoelectret, thermistor or radio frequency mechanism has sparked intensive scientific interest in recent years [13–16]. Such a smart face mask is a meaningful application in clinical therapeutics and daily prevention in minimising exposure to COVID-19 viruses and other environmental hazards. The waveforms of signals play essential roles in judging health condition. For example, a deep analysis to electroencephalograms (EEGs) and electrocardiograms (ECGs) could provide significative information of the electrical activity of the brain and heart, respectively [17,18]. Despite previously reported classes of smart face masks which enable the real-time monitoring of human breath rate, these masks do not consider the waveform of the response signal and hence cannot satisfactorily reveal the physical condition to the same extent as the EEG and ECG signals.

A typical smart face mask primarily consists of a sensing unit, a signal reading circuit, and a control chip. The gained digital signals are transmitted to the computer or a smartphone in wired or wireless way. To fit on the surface of the mask and properly generate the response signal for human breath, the sensing unit should be mechanically flexible, breathing-airflow sensitive, and long-term stable. Typically, the working principles of breath sensors include radio-frequency, capacitance, piezoelectricity, triboelectricity, and resistance. For instance, a multiscale porous organic substrate is printed with silver nanowires (AgNWs) *via* spray printing to construct a radio frequency harmonic transponder. A face mask configured with this transponder enables the monitor of cough and mask-wearing state simply [13,14,16,19–22]. Resistive-type sensors present several advantages over other types, including simple classes of materials, convenient manufacturing routes, and straightforward measurement methods, which meet the requirements of monitoring systems with minimum expenditure [23–26]. Additionally, the waveform generated by the resistive-type sensors is smoother than that of others, which can deliver more details of the human breath. Currently, sensors based on silicon, ZnO, reduced graphene oxide (rGO), and other resistive-type materials are employed in breath monitoring. For example, based on the piezoresistive principle, the chemically etched Si nanorod arrays were manufactured and demonstrated in sensing human breath. However, there are still some problems that have not been solved. One is the multi-functional sensing ability of the sensor to various human respiratory statuses, while the other is continuous and long-term dynamic breathing process monitoring capacity [27–29].

Transition metal perovskite oxides are another type of sensor materials which can show a range of useful responses. Owing to the strong coupling among spin, charge, orbital, and lattice degrees of freedom in them, many fascinating physical properties such as superconducting, half-metallic, ferromagnetic, ferroelectric, multiferroic, etc, are present [30–39]. The half-metallic perovskite manganite oxides are particularly attractive because of their diverse physical phenomena including (anti-) ferromagnetism (FM), colossal magnetoresistance (CMR), metal-insulator transition (MIT), etc [40–42]. For example, $La_{0.7}Sr_{0.3}MnO_3$ (LSMO) has been widely investigated because of its high Curie temperature among the manganites ($T_C \sim 360$ K for bulk) and almost full spin polarization at the Fermi level, which can be used for designing novel electronic devices[43–45]. LSMO have been widely employed in designing functional sensors, such as pressure sensor [46], chemical sensor [47], humidity sensor [48] and strain sensor [49]. However, there is no special work reporting flexible and wearable LSMO film as a human breath sensor. In addition, owing to the manganites and Mica without toxicity, magnetic nanoparticles based on manganite perovskite ($La_{1-x}Sr_xMnO_3$) have been widely utilized in various biomedical applications, including therapeutic and diagnostic applications, *e.g.*, magnetic hyperthermia therapy (MHT) and magnetic resonance imaging (MRI) for the treatment of cancers [50]. Therefore, the LSMO and Mica are very suitable materials for fabricating biocompatible sensors.

In this work, we design a wearable human breath-monitoring face mask by utilizing flexible LSMO/Mica sensor. The sensor shows long-time response signals, demonstrating the system's stable, restorable, and endurable sensing ability when monitoring different breath modes, *i.e.*, cough, normal breath, and deep breath. We find the breath strength and breath rate increase as human exercise intensity increases, according to the results of the analysis of breath intensity, breath rate and the shape of response signals. A combination of original signal waveform, statistical breath intensity and breath rate offers the possibility to detect abnormalities of the respiratory system. Furthermore, by comparing simulated and experimental data, we confirm that thermal diffusion in LSMO under the influence of breath airflow is responsible for the change of resistance in flexible LSMO/Mica sensor during monitoring human breath. Moreover, both simulated and experimental results demonstrate good discernibility of flexible LSMO/Mica sensors for the applications of monitoring different breath modes.

2. Results and discussions

We firstly fabricated LSMO thin films on flexible Mica substrates by employing pulsed laser deposition with sintered LSMO target (Fig. S1). High crystallinity LSMO thin films were epitaxially grown on Mica substrates, according to the results of structural characterizations including X-ray diffraction (XRD), high-resolution transmission electron microscopy (HRTEM), and atomic force microscopy (AFM) (Fig. S2). Moreover, the orientation relationship is determined to be LSMO [110] || Mica [001] and LSMO [1–11] || Mica [060], which is consistent with previous work [51]. Besides, flexible LSMO/Mica thin films exhibit exceptional resistance stability as a function of mechanical bending cycles up to 50,000 with the temperature ranging from 15 ℃ to 45 ℃ under a bending radius of 5 mm. (Fig. S3), in comparable to other reports [52,53]. These results indicate that the change of electrical resistance caused by the temperature variation through human exhalation and inhalation can be detected and recognized in human breath monitoring.

Fig. 1 depicts the roadmap of human breath monitoring systems. Reliable signal transmission is highly desired in clinical monitoring to continuously monitor the patient's breath condition, therefore, the wired scheme is the optimum option for clinical monitoring due to its reliability. However, portability is highly needed in daily monitoring, when the wireless scheme triumphs over the wired scheme in a human breath-monitoring system [19,54]. Hence, we designed both wired and wireless monitoring modes for flexible LSMO/Mica sensors in human breath monitoring. As a sensor, a flexible LSMO/Mica thin film was mounted on the inner side of a face mask using double-sided adhesive tape (Fig. S4). Fig. 1b displays the schematic diagram of daily monitoring mode (or wireless mode) of flexible LSMO/Mica sensor. In wireless mode, a flexible LSMO/Mica sensor was connected to a compact integrated circuit by the 4-wire resistance measurement method. The

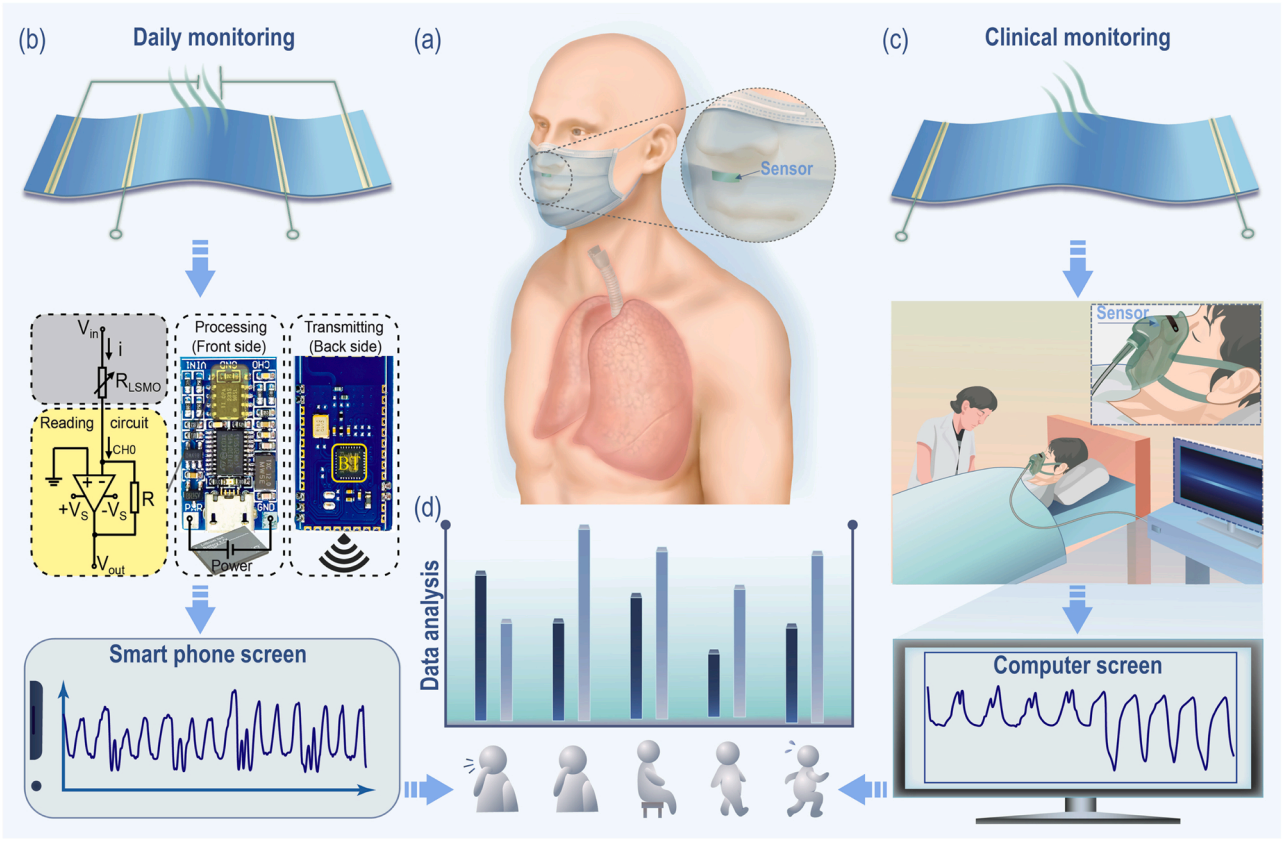

Fig. 1. Implementation roadmap of human breath monitoring systems. a) Schematic diagram of monitoring human breath by utilizing manganite oxide respiration sensor. Schematic diagrams of b) the wireless mode and c) the wired mode of LSMO/Mica sensors used in human breath monitoring. d) The obtained data is for further processing and analysis.

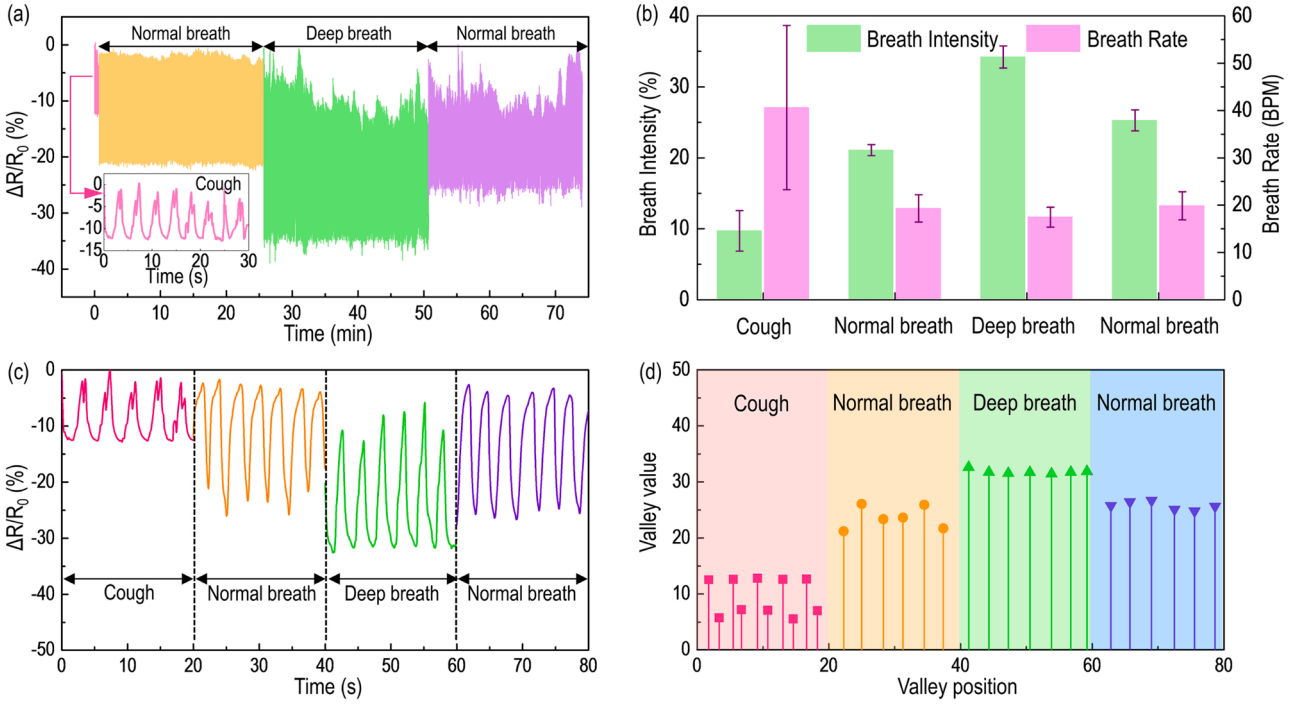

Fig. 2. a) The change of electrical resistance in flexible LSMO/Mica sensor *versus* time obtained at the breath modes of cough (inset), normal breath, deep breath, and back to normal breath. b) The change of breath intensity and breath rate obtained at the breath modes of cough, normal breath, deep breath, and normal breath. c) Magnifying waveform for each kind of breath mode and d) corresponding distribution diagram of valley value (defined as $-\Delta R/R_0$) and valley positions (points in time).

response signals were directly shown on smartphone screens to provide information about human breath conditions. Fig. 1c schematically illustrates the clinical monitoring mode (or wired mode) of our flexible LSMO/Mica sensor. In this mode, the flexible LSMO/Mica sensor was directly connected to the flexible device analysis system (AES-4SD, SINO AGGTECH) platform using the 2-wire method. The AES-4SD system simultaneously serves as both current source and voltage readout, and calculates the resistance, and then displays the response signals on a computer screen. Afterwards, the measured data could be further processed and analyzed for providing proper suggestions for human health care and treatment (Fig. 1d).

Good repeatability is an essential characteristic in assessing the quality of a breath monitoring system, especially for the measurements of common and perennial chronic respiratory diseases [21,55,56]. Therefore, we conducted long-term tests to examine the stability of response to actual breath in clinical monitoring mode under different breath status, *i.e.*, cough, normal breath, and deep breath. The response signals as a function of time are plotted in Fig. 2a. For the flexible LSMO/Mica sensor described here, R_0 is the initial resistance, ΔR is the change of resistance under various breath statuses, and $\Delta R/R_0$ is defined as the percent change in resistance for quantizing response results. Excellent repeatability were observed in continuous breath monitoring (or normal breath) for at least 3 h (Fig. S5), which is comparable to other reports [13,57]. The value of $\Delta R/R_0$ distinctively alters in lockstep with the breath state, from cough to normal breath to deep breath. Note that after the deep breath the response signal of normal breath couldn't recover to its initial state at a certain level. This could be attributable to the change in humidity gathered on the surface of flexible LSMO/Mica sensor caused by exhalation and inhalation [48].

Fig. 2b presents the statistical data of breath intensity (defined as $\Delta R/R_0$) and breath rate (beats per minute, BPM) under various breath status. The breath intensity of cough, normal breath, deep breath, and back to normal breath is around 9.70 ± 2.84%, 21.09 ± 0.77%, 34.22 ± 1.57%, and 25.28 ± 1.48%, respectively. A cough presents a lower breath intensity than the others, while a deep breath has the highest value among these breath statuses. The breath rate of cough, normal breath, deep breath, and back to normal breath is estimated to be around 40.62 ± 17.38, 19.30 ± 2.88, 17.45 ± 2.09, and 19.86 ± 2.98 BPM, agreeing well with the previous report [58]. A cough shows the highest breath rate among these breath statuses, which is in accordance with the previous study [13]. However, there is no discernible difference in rate between normal breath and deep breath. This makes sense considering that the tester is merely breathing deeper rather than quicker. Moreover, we found that the normal breath rates before and after deep breath are almost equivalent, suggesting the exceptional repeatability of the flexible LSMO/Mica sensor in breath monitoring. A magnified view of the details of response signals is further shown in Fig. 2c, indicating an excellent sensing ability of flexible LSMO/Mica sensor for human breath. Furthermore, the corresponding distribution diagram of valley value (defined as the local minimum magnitude of $-\Delta R/R_0$) and valley position (defined as points in time) is summarized in Fig. 2d. Clearly, different breath status presents unique shapes and disparate ranges in their response signals. Within each period, the cough signal exhibits a characteristic bimodal-peak waveform, whereas other breath status only presents a single-peak waveform [22]. Although the rate of coughing was higher than that of other breath status, the intensity was significantly lower since the lungs need to shrink twice for each period and hence can't recover to their initial state. Altogether, these results collectively indicate that flexible LSMO/Mica sensor exhibits splendid discernibility of various breath status in continuous, long-term monitoring of the dynamic breathing process.

To demonstrate the portability of LSMO in breath monitoring, a wireless human breath-monitoring face mask containing a flexible LSMO/Mica sensor and a wireless signal processing module was designed, as illustrated in Fig. 3a. The change of resistance in analog signals of the flexible LSMO/Mica sensor to the breath is converted into digital signals under the operation of the wireless signal processing module and transmitted to the smartphone by Bluetooth (Fig. 1b and Fig. S4). In practice, the working current is only around 10 mA for the processing module and 0.1 mA for flexible LSMO/Mica sensor. Hence, it is expected that the face mask can work for dozens of hours with an attached fully charged 300-mAh lithium battery, enough for daily

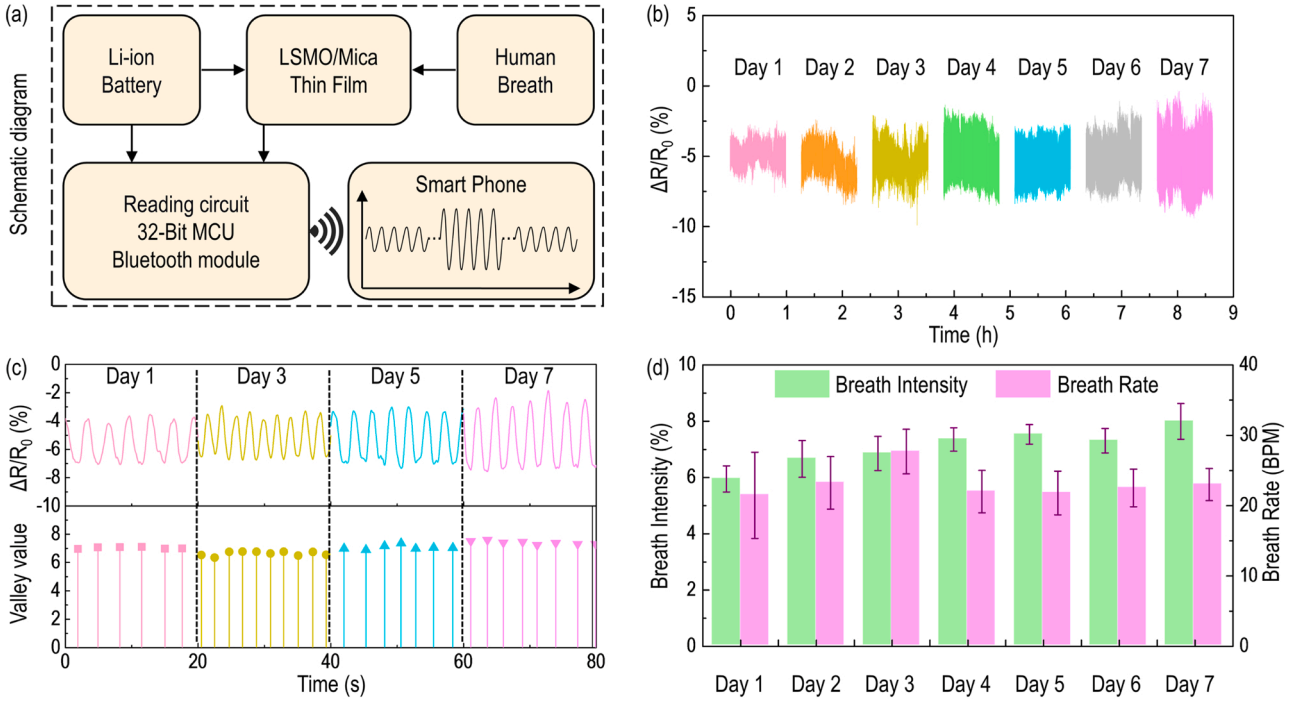

Fig. 3. a) Schematic diagram of the wireless human breath monitoring module. b) The stability of flexible LSMO/Mica sensor for human breath at sitting mode recorded within one week. c) Top panel: magnification of waveform of day 1, day 3, day 5, and day 7. Bottom panel: corresponding distribution diagram of valley value ($-\Delta R/R_0$) and valley positions (time). d) Statistical histogram of breath intensity and rates obtained from day 1 to day 7.

monitoring. An endurance test was performed to investigate the long-term responding stability. Fig. 3b shows the response signals of human breath *versus* time for one hour every day within one week, which were recorded at human static (sitting) status. Magnified views of the waveform measured from day 1, day 3, day 5, day 7, and their corresponding distribution diagram of valley value and valley position are presented in Fig. 3c. We observed fairly stable and restorable response signals generated from the flexible LSMO/Mica sensor. Additionally, Fig. 3d statistically summarizes the data of breath intensity and rate that was gathered from days 1 to day 7. The long-term stability of the wireless mode is clearly demonstrated by a stable breath intensity and rate, which is comparable to the previous study [20]. This robust sensing behaviour can be attributed to the excellent electrical transport property of flexible LSMO/Mica sensor. On the other hand, at a micro level, by comparing Fig. 3b with Fig. 3d, we can see that the breath intensities of days 4–7 are a little higher than that of days 1–3, while the breath rates of days 4–7 are a little lower than that of days 1–3. This may be due to the fluctuation in the breathing state of the tester at different dates to a certain extent, *i.e.*, breathing a little lighter and faster or a little deeper and slower. In addition, under a sudden sneeze, the LSMO/Mica sensor shows a response within 0.1 s (Fig. S6), indicating it can work normally under a high-speed impact. Also, the sensing ability of the LSMO/Mica sensor is not damaged after sanitizing with medical alcohol (Fig. S7).

To explore the individual differences in respiratory behaviours with application of the flexible LSMO/Mica sensor operating under a wireless mode [59]. two volunteers (Tester #1 or T_1, Male; Tester #2 or T_2, Female) were recruited to perform the following tests. Different moving speeds on a treadmill, *i.e.*, 0 KPH (kilometres per hour), 3 KPH, 6 KPH, and 9 KPH were defined as the modes of sitting, walking, jogging, and running, respectively. The breath signals wirelessly transmitted from a breath-monitoring face mask are shown in Fig. 4a. Obviously, different intensities of exercises induce different values of $\Delta R/R_0$. Statistical histograms of breath intensity and rate for T_1 and T_2 under different modes are summarized in Fig. 4b. The data collected from the male and female presents a similar trend when moving speeds increase [60]. For T_1, breath intensities of walking, jogging, and running were around $6.70 \pm 0.27\%$, $13.34 \pm 1.08\%$, and $14.09 \pm 1.10\%$, respectively, and his corresponding breath rates were around 20.40 ± 4.54, 25.45 ± 5.84, and 27.17 ± 4.97 BPM. Note that T_1 increases the oxygen uptake rate by enormously increasing the breath intensity and slightly increasing breath rate to accommodate the exercise strength. This means deeper breath might be more acceptable for T_1. For T_2, breath intensities were around $7.28 \pm 0.58\%$, $12.22 \pm 1.20\%$, and $10.97 \pm 0.76\%$, and her corresponding breath rates were around 18.64 ± 6.00, 21.28 ± 4.03 and 39.87 ± 2.78 BPM for walking, jogging, and running, respectively.

We observed a similar tendency as T_1 at low exercise strength ($\leqq 6$ KPH). However, the breath intensity decreases and breath rate increases as the exercise strength increases to 9 KPH, indicating that T_2 prefers to increase the breath rate than breath intensity for promoting the intake of oxygen. The breath rate-time curves (Fig. S8) also clearly reveal these differences between the testers. It should also be mentioned that T_1 suffered from airway hyperresponsiveness (AHR) two years ago, which is a state characterized by easily triggered bronchospasm (contraction of the bronchioles or small airways) [61]. Consequently, for the sitting status as shown in **Fig. 4**b, T_1 presented a little lower breath intensity ($7.82 \pm 0.46\%$) than that of T_2 ($9.78 \pm 0.87\%$), but his breath rate (23.92 ± 2.19 BPM) was much higher than that of T_2 (13.40 ± 4.27 BPM), and was also little higher than that of a healthy person [7,58]. The magnifying waveform of breath and the corresponding distribution diagram of the valley value and valley position for T_1 and T_2 are further displayed in Fig. 4c–d, also supporting the same conclusions. Furthermore, take running state of T_2 for exampling (Fig. S9), which presents the highest breath rate, the response/recovery time of 0.7 s/0.7 s is fast enough to generate accurate signal to human breath. Overall, these results strongly support that our wireless face masks based on flexible LSMO/Mica sensors possess distinguished stability and multi-modal advantages in capturing clinic meaningful information from continuous, long-term monitoring of the dynamic human breath. In addition, the experimental results (Fig. 2b, Fig. 3d and Fig. 4b) reveal that the common range of breath rate of human breath is about 15–45 BPM), *i.e.*,

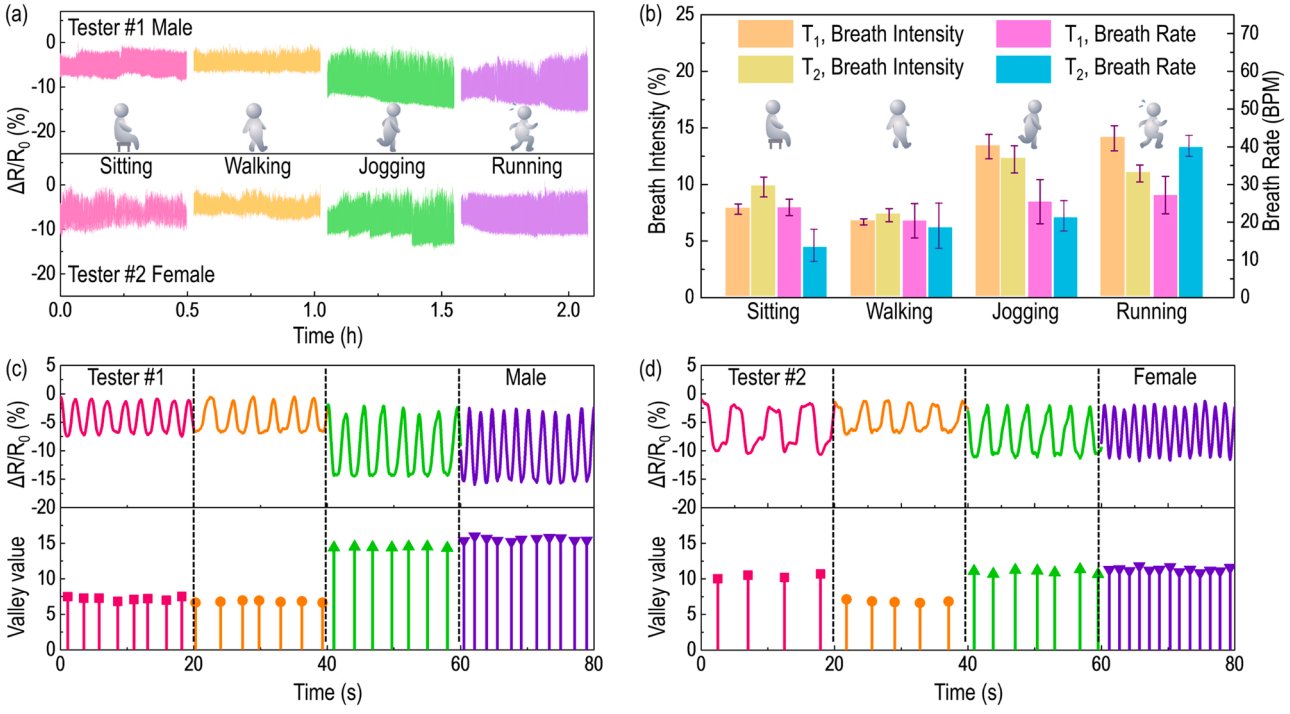

Fig. 4. a) The change of resistance *versus* time at different modes tested by male (tester #1, top panel) and female (tester #2, bottom panel). b) Statistical histogram of breath intensity and rates at different modes obtained from tester #1 (T_1, male) and tester #2 (T_2, female). c-d) Magnification of waveform measured at different modes and its corresponding distribution diagram of valley value ($-\Delta R/R_0$) and valley position (time).

less than 4 s for each breath cycle. The fluctuation in ambient temperature caused by the different motion modes is not periodic and has a much longer variation period than that of breathing. On the other hand, the LSMO/Mica respiration sensor mounted on the face mask is close to the nose and mouth. Therefore, the response signals of the LSMO/Mica respiration sensor result from the temperature variation of respiratory airflow rather than that of the human body.

We have experimentally confirmed the thermoresistance response of our LSMO/Mica sensor to temperature variation (Fig. S3). To clarify how the thermal flow affects the electrical resistivity of the LSMO/Mica sensor and to gain insight into the correlation between the thermal distribution and the resistance change in the flexible LSMO/Mica sensor, we performed a finite element analysis (FEA) using the COMSOL Multiphysics software. A rectangular flexible LSMO/Mica sensor was placed at the centre of an area that was exposed to the breath airflow. The simulation was conducted to present a 2D cross-sectional views of the temperature change of the sensor and its surrounding environment, with the exhale breath flowing vertically downwards from the top of the view, and inhale breath flowing the opposite way. Different breath modes possessed distinctive flowing patterns, *e.g.* normal breath had exhale and inhale flowing speed of up to 2 m/s at a rate of 10/min, deep breath had the same exhale and inhale speed but a slower rate of 6/min, while cough presented a higher exhale speed of up to 6 m/s with a much more intensive rate. It was simulated that the exhale breath would bring warmer air to the surrounding area while inhale breath would vacuum such warm air to let cooler air in, thus to change the temperature of the LSMO sensor through heat conduction. Fig. 5a provides typical images for the thermal distribution at the cross-section of LSMOs at their highest heated-up status under different breath modes, *i.e.*, initial state, normal breath (Movie S1), deep breath (Movie S2), and cough (Movie S3). The temperature field was uniformly distributed on the cross-sectional area of LSMO at the initial state and presented differences after being subjected to various breath airflow. For quantizing the average discrepancies among these situations, an averaged value of cross-sectional temperature variations (ΔT) was determined to be 0 K for initial state, while 0.60 K for normal breath, 1.04 K for deep breath, and 0.56 K for cough. We found that the temperature variation at the left and right edges of the rectangular LSMO is higher, which might be due to the difference in thermal conductivity. According to previous reports [62–64], the thermal conductivity of LSMO (1–3 W/m·K) and Mica (~ 0.5 W/m·K) is substantially higher than that of air (~ 0.026 W/m·K), resulting in difficulty for heat dissipation at the edges of LSMO than its middle.

Supplementary material related to this article can be found online at doi:10.1016/j.nanoen.2023.108460.

Simulated and experimental ΔT are further compared and summarized in Fig. 5b and Fig. S10. Where, simulated ΔT is obtained from the COMSOL data, while experimental ΔT is estimated calculated from real breath signals (Fig. 2) and electrical resistivity of LSMO (Fig. S3b). It can be seen that normal breath and deep breath modes are clearly distinguished in both simulation and experiment. The value of ΔT in the deep breath mode is higher than that of normal breath mode, revealing the responsiveness of flexible LSMO/Mica sensor for different human breath modes. To further understand dynamic response signals to warm air flow, simulated and experimental cough modes were designed, including coughing once, twice, and thrice in a whole breath period, which were named as single-cough, double-cough, and triple-cough. The simulation airflow, simulation averaged sensor temperature and experimental response signals ($\Delta R/R_0$) exhibit a good agreement with each other, as depicted in Fig. 5c. A positive and a negative flow rate represented the exhale and the inhale from a breath, respectively. Furthermore, these three cough statuses generated 1/2/3 sharp falling edges in the response signals ($\Delta R/R_0$), which are the crucial features for distinguishing a cough from a normal breath. The simulated ΔT was

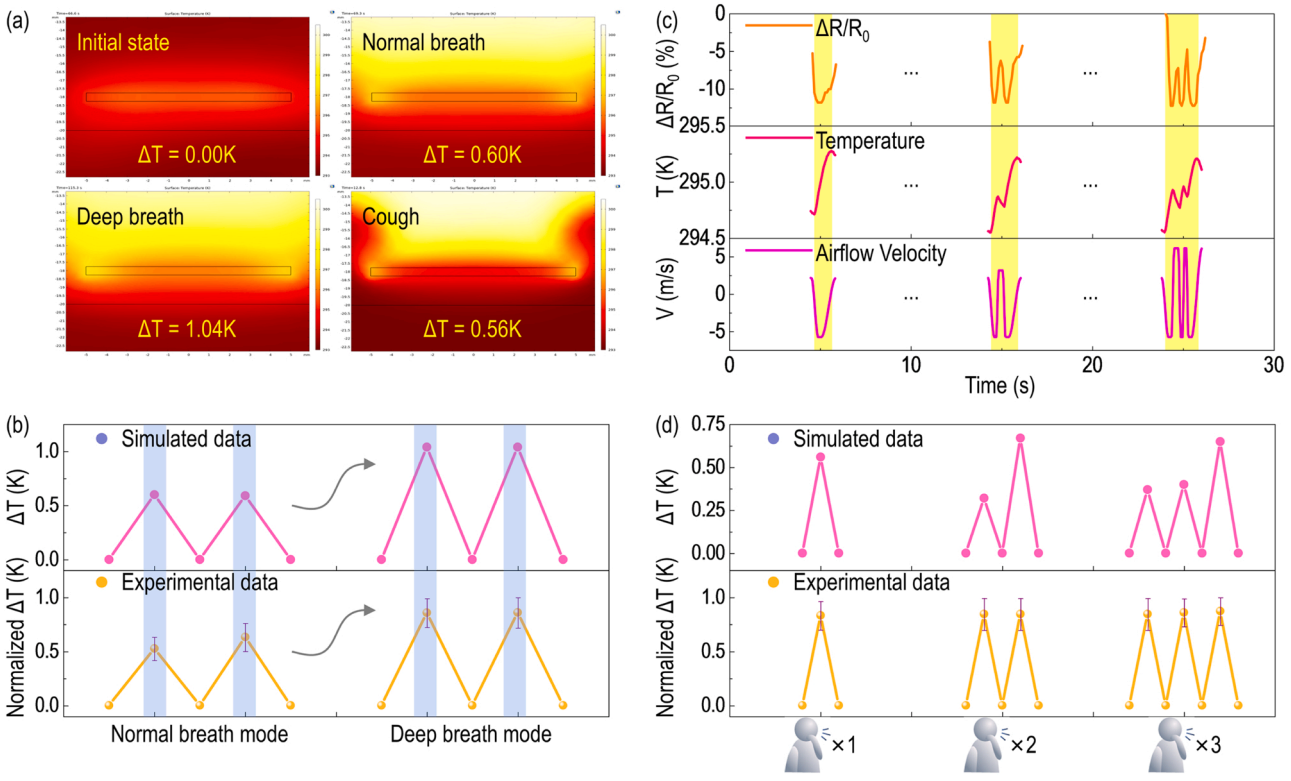

Fig. 5. a) The temperature field distribution simulated in flexible LSMO/Mica sensor at its highest heated-up status obtained at different breath states. b) The change of temperature in flexible LSMO/Mica sensor at normal breath and deep breath obtained from simulation (top panel) and experiment (bottom panel). c) Correlation among experimental response signals of human breath, simulated temperature variations, and airflow velocity (predefined for simulation). d) The change of temperature in flexible LSMO/Mica sensor at single-, double-, and triple-cough obtained from simulation (top panel) and experiment (bottom panel).

further compared to the experimental ΔT, as presented in Fig. 5d. Different coughs were clearly distinguished according to both simulated and experimental results. Based on the simulated results, we determined that the resistance change in a flexible LSMO/Mica sensor is caused by the thermal distribution from mouth. More importantly, these results strongly indicate good responsiveness and discernibility of our flexible LSMO/Mica sensor for different human breath modes.

3. Conclusion

In conclusion, we have fabricated high-quality flexible and inorganic epitaxial LSMO thin film on a flexible Mica substrate, which was integrated as a sensor in a human breath-monitoring face mask. Two kinds of application scenarios were tested to investigate and demonstrate the feasibility of flexible LSMO/Mica sensor in monitoring human breath. The detected signals from the breath were accessed and viewed on a smartphone or computer in real time. The sensing system presented outstanding stability and a multi-modal capability in continuous, long-time monitoring of the dynamic human breath. By using our smart masks, breath parameters from the disparate breath situations of humans of different genders were further analyzed and discussed, revealing the differences in breath modes between male and female. In addition, supported by COMSOL simulation, we determined that the temperature distribution in LSMO under the influence of a breath airflow is responsible for the change of resistance in the flexible LSMO/Mica sensor during the measurements of the human breath. More importantly, both simulated and experimental results demonstrated good discernibility of the flexible LSMO/Mica sensor for different breath modes. Our work provides a new pathway to design flexible and wearable human breath-monitoring face masks to detect possible abnormalities of the respiratory system, with meaningful applications in clinical and daily monitoring.

4. Methods

4.1. Thin film fabrication

Fluorophlogopite mica (F-Mica) is a kind of flexible substrate that has been extensively utilized in the deposition of functional oxides. $La_{0.7}Sr_{0.3}MnO_3$ (LSMO) thin films were directly deposited on Mica (Changchun Taiyuan Fluorophlogopite Co., China) substrates using a PLD system coupled to a KrF excimer laser (COMPexPRO 205 F, $\lambda = 248$ nm, Coherent Inc.) operating at a laser intensity of 1.5 $J{\cdot}cm^{-2}$ and a pulse frequency of 4 Hz. The manufacturing process of polycrystalline LSMO target used in this study was covered in our earlier paper [65]. The optimal conditions for epitaxial development of LSMO were a substrate temperature of 700 ℃ and a partial pressure of 0.1 mbar. Highly-pure nitrogen gas flow was used to form a (110)-oriented LSMO seed layer[51], and then highly-pure oxygen gas was replaced the nitrogen to grow LSMO film. The PLD chamber spontaneously cooled to room temperature after the completion of film deposition.

4.2. Properties characterization

The crystal nature of $La_{0.7}Sr_{0.3}MnO_3$/Mica heterostructures was identified by an X-ray diffractometer (Empyrean, Malvern Panalytical) configured with Cu K_α radiation ($\lambda = 1.5406$ Å). The surface topography of $La_{0.7}Sr_{0.3}MnO_3$/Mica heterostructures was examined by Atomic Force Microscope (AFM, Asylum Research MFP-3D, Oxford Instruments), which was working at tapping mode with an AC240TS-R3 probe (70–75KHz, Olympus Corporation). The microstructure of $La_{0.7}Sr_{0.3}MnO_3$/Mica heterostructures was characterized by Transmission Electron Microscope (TEM, Thermo Fisher Scientific TALOS F200X), which was operated at 200KV. Transport properties (ρ(T) curves) of the $La_{0.7}Sr_{0.3}MnO_3$/Mica heterostructures were measured by using Physical Property Measurement System (PPMS, QD). $La_{0.7}Sr_{0.3}MnO_3$/Mica heterostructure was mechanically exfoliated, cut into a rectangle shape (10 mm × 3 mm), and placed on the Flexible Device Analysis System (AES-4 SD, SINO AGGTECH) platform for studying the mechanical flexibility. Silver conductive epoxy and platinum wire were used to connect $La_{0.7}Sr_{0.3}MnO_3$/Mica thin films and measurement units by the 2-wire method. Using the percent change of electrical resistance $\Delta R/R_0$ to characterize the response of the $La_{0.7}Sr_{0.3}MnO_3$/Mica heterostructure to different stimulation (ΔR and R_0 are the resistance change and the initial resistance value of $La_{0.7}Sr_{0.3}MnO_3$).

4.3. Sensor design

Two kinds of application scenarios, including clinical monitoring mode and daily monitoring mode, were designed and investigated to demonstrate breath monitoring. For pursuing the stability of signal transmission in simulating the clinical monitoring mode (*i.e.* wired mode), the flexible LSMO/Mica sensor (10 mm × 3 mm) was attached to the inner side of the face mask with double-sided adhesive tape and connected with an AES-4 SD system by the 2-wire method to test the monitoring capacity for human breath. In the daily monitoring mode (*i.e.* wireless mode), an integrated circuit board containing a MOS-FET, an operational amplifier, a crystal oscillator, an analog-to-digital (A/D) converter, a 32-bit microcontroller unit (MCU), and a Bluetooth (BT) module was used to obtain and transmit signals. Similarly, flexible LSMO/Mica thin film (10 mm × 3 mm) was mounted on the inner side of the face mask using double-sided adhesive tape, but, the connection to the integrated circuit was the 4-wire method. The collected breath data was wirelessly transmitted *via* Bluetooth and displayed on a smartphone screen in real time. Informed consent for experimentation with volunteers was obtained prior to their participation in this study. Specially, the methodology of acquiring breath rate-time (such as Fig. S5b) from breath signals (as shown in Fig. S5a) is showed in Fig. S11. In a $\Delta R/R_0$-time curve, we define the valley position of each breath cycle as.

$t_1, t_2, t_3, \ldots, t_n, t_{n+1}, \ldots$

hence the total time for a breath cycle at moment t_n is,

$\Delta t_n = t_n - t_{n-1}$,

then, the corresponding breath rate at this moment is,

$60/\Delta t_n$ (unit: BPM)

Finally, we can calculate breath rate within 1/10/20 or any breath cycles as required. In this work, calculating breath rate every 20 breath cycles makes a good appearance in the breath rate-time curve, just like the heart rate curve acquired by a commercial smart bracelet.

4.4. COMSOL simulation

Conjugate heat transfer with laminar flow multiphysics module was adopted for simulating the thermal conductance between breath flow and the sensor. A 2D mode was used to study the cross-section view of the sensor and its surrounding atmosphere. The sensor had dimensions of 10 mm long and 0.5 mm thick, with a heat capacity set at 550 J/(kg·K) referred from experimental data[66]. LSMO sensor was located at the center of a considerable trapezoidal area, which was assigned to be filled with air. The top edge of the trapezoid was made the inlet of the airflow (representing the "mouth") with temperature set at 37 ºC, which could be imposed with various flow rates including positive rates standing for exhaling and negative for inhaling. And the bottom edge of the trapezoid was made the outlet with freedom of airflow with temperature set at 20 ºC, whereas the side edges of the trapezoid area were set to be thermal insulated for proximity. The LSMO sensor was located approximately 17.5 mm away from the top inlet edge. A "time--dependent" study was used with time-related breath rate curves for

mimicking normal breath, deep breath and coughs. Average temperatures of the cross-section areas of the sensor were calculated under different breath conditions.

CRediT authorship contribution statement

Lianxu Ye: date curation, formal analysis, investigation, methodology, writing-review & editing, **Fan Wu:** date curation, formal analysis, investigation, methodology, **Ruixing Xu:** date curation, formal analysis, investigation, methodology, **Di Zhang:** date curation, formal analysis, investigation, methodology, **Juanjuan Lu:** date curation, formal analysis, investigation, methodology, **Chuanlong Wang:** date curation, formal analysis, investigation, methodology, **Anjiang Dong:** date curation, formal analysis, investigation, methodology, **Sichen Xu:** date curation, formal analysis, investigation, methodology, **Lejun Xue:** date curation, formal analysis, investigation, methodology, **Zixin Fan:** date curation, formal analysis, investigation, methodology, **Longjie Xu:** date curation, formal analysis, investigation, methodology, **Kaifeng Li:** date curation, formal analysis, investigation, methodology, **Dong Li:** date curation, formal analysis, investigation, methodology, **Ahmed Kursumovic:** funding acquisition, writing-review & editing, **Run Zhao:** date curation, formal analysis, investigation, methodology, **Rujun Tang:** date curation, formal analysis, investigation, methodology, **Lei Qiu:** date curation, formal analysis, investigation, methodology, software, **Haiyan Wang:** date curation, formal analysis, investigation, methodology, funding acquisition, writing-review & editing, **Judith L. MacManus-Driscoll:** funding acquisition, writing-review & editing, **Qingshen Jing:** conceptuatlization, project administration, software, date curation, methodology, writing-original draft, writing-review & editing, **Weiwei Li:** funding acquisition, conceptuatlization, project administration, supervision, writing-original draft, writing-review & editing, **Hao Yang:** funding acquisition, conceptuatlization, project administration, supervision, writing-review & editing.

Declaration of Competing Interest

The authors declare that they have no known competing financial interests or personal relationships that could have appeared to influence the work reported in this paper.

Data availability

Data will be made available on request.

Acknowledgements

H.Y. acknowledges support from the National Natural Science Foundation of China (Grant No. 52172269, 92163102). W.-W.L. acknowledges support from the National Natural Science Foundation of China (Grant No. 52102177), the National Natural Science Foundation of Jiangsu Province (Grant No. BK20210313), Top-notch Academic Programs Project of Jiangsu Higher Education Institutions (TAPP), and the Jiangsu Specially-Appointed Professor Program. The research work is supported by the supporting funds for talents of Nanjing University of Aeronautics and Astronautics. D. Z., J. L. and H.W. acknowledge the support from the U.S. Department of Energy, Office of Science, Basic Energy Sciences under Award DE-SC0020077 and the U.S. National Science Foundation under Award DMR-2016453 and DMR-1809520 for the TEM and HRTEM work at Purdue University. J.L.M-D. thanks the EU-H2020-ERC-ADG # 882929 EROS grant, and the Royal Academy of Engineering Chair in Emerging Technologies grant, CIET1819_24. A.K. acknowledges support from the Leverhulme Trust grant, RPG-2020-041.

Appendix A. Supporting information

Supplementary data associated with this article can be found in the online version at doi:10.1016/j.nanoen.2023.108460.

References

[1] H.D. Li, X.C. Zhao, Y.J. Wang, X. Lou, S.Z. Chen, H. Deng, L. Shi, J.S. Xie, D. Z. Tang, J.P. Zhao, L.S. Bouchard, L.M. Xia, X. Zhou, Sci. Adv. 7 (2021) 1–9, https://doi.org/10.1126/sciadv.abc8180.
[2] P. Horby, W.S. Lim, J.R. Emberson, M. Mafham, J.L. Bell, L. Linsell, N. Staplin, C. Brightling, A. Ustianowski, E. Elmahi, B. Prudon, C. Green, T. Felton, D. Chadwick, K. Rege, C. Fegan, L.C. Chappell, S.N. Faust, T. Jaki, K. Jeffery, A. Montgomery, K. Rowan, E. Juszczak, J.K. Baillie, R. Haynes, M.J. Landray, R. C. Grp, N. Engl. J. Med 384 (2021) 693–704, https://doi.org/10.1056/NEJMoa2021436.
[3] D.J. Miller, J.V. Capodilupo, M. Lastella, C. Sargent, G.D. Roach, V.H. Lee, E. R. Capodilupo, PLoS One 15 (2020) 1–10, https://doi.org/10.1371/journal.pone.0243693.
[4] K. Vaporidi, E. Akoumianaki, I. Telias, E.C. Goligher, L. Brochard, D. Georgopoulos, Am. J. Respir. Crit. Care Med 201 (2020) 20–32, https://doi.org/10.1164/rccm.201903-0596SO.
[5] J.D. Power, C.J. Lynch, M.J. Dubin, B.M. Silver, A. Martin, R.M. Jones, NeuroImage 204 (2020), 116234, https://doi.org/10.1016/j.neuroimage.2019.116234.
[6] M.A. Cretikos, R. Bellomo, K. Hillman, J. Chen, S. Finfer, A. Flabouris, Med. J. Aust. 188 (2008) 657–659, https://doi.org/10.5694/j.1326-5377.2008.tb02163.x.
[7] A. Natarajan, H.W. Su, C. Heneghan, L. Blunt, C. O'Connor, L. Niehaus, NPJ Digit. Med. 4 (2021) 1–10, https://doi.org/10.1038/s41746-021-00493-6.
[8] H. Endoh, S. Yamaguchi, Y. Hayashi, S. Ohhashi, T. Honda, M. Nitta, H. Honda, Crit. Care Med 41 (2013) 577, https://doi.org/10.1097/01.ccm.0000439818.36331.58.
[9] P. Fathizadeh, W.C. Shoemaker, C.C.J. Wo, J. Colombo, Crit. Care Med 32 (2004) 1300–1305, https://doi.org/10.1097/01.CCM.0000127776.78490.E4.
[10] A. Tong, A. Baumgart, N. Evangelidis, A.K. Viecelli, S.A. Carter, L.C. Azevedo, T. Cooper, A. Bersten, L. Cervantes, D.P. Chew, S. Crowe, I.S. Douglas, E. Flemyng, J.H. Elliott, E. Hannan, P. Horby, M. Howell, A. Ju, J. Lee, E. Lorca, D. Lynch, K. E. Manera, J.C. Marshall, A.M. Gonzalez, A. McKenzie, S. Mehta, M. Mer, A. C. Morris, D.M. Needham, S. Nseir, P. Povoa, M. Reid, Y. Sakr, N. Shen, A.R. Smyth, A.J. Simpson, T. Snelling, G.F.M. Strippoli, A. Teixeira-Pinto, A. Torres, T. Turner, S. Webb, P.R. Williamson, L. Woc-Colburn, J.H. Zhang, J.C. Craig, C.C.O.S. Investi, Crit. Care Med 49 (2021) 503–516, https://doi.org/10.1097/CCM.0000000000004817.
[11] M. Brabrand, P. Hallas, L. Folkestad, C.H. Lautrup-Larsen, J.B. Brodersen, J. Crit. Care 44 (2018) 404–406, https://doi.org/10.1016/j.jcrc.2017.12.020.
[12] D.K. Chu, E.A. Akl, S. Duda, K. Solo, S. Yaacoub, H.J. Schunemann, Lancet 395 (2020) 1973–1987, https://doi.org/10.1016/S0140-6736(20)31142-9.
[13] J.W. Zhong, Z.Y. Li, M. Takakuwa, D. Inoue, D. Hashizume, Z. Jiang, Y.J. Shi, L. X. Ou, M.O.G. Nayeem, S. Umezu, K. Fukuda, T. Someya, Adv. Mater. 34 (2022) 1–10, https://doi.org/10.1002/adma.202107758.
[14] M. Lazaro, A. Lazaro, R. Villarino, D. Girbau, Sensors 21 (2021) 1–28, https://doi.org/10.3390/s21227472.
[15] Y.L. Cheng, C.Y. Wang, J.W. Zhong, S.Z. Lin, Y.J. Xiao, Q.Z. Zhong, H.L. Jiang, N. Wu, W.B. Li, S.W. Chen, B. Wang, Y.Y. Zhang, J. Zhou, Nano Energy 34 (2017) 562–569, https://doi.org/10.1016/j.nanoen.2017.03.011.
[16] Z.L. Ye, Y. Ling, M.Y. Yang, Y.D. Xu, L. Zhu, Z. Yan, P.Y. Chen, ACS Nano 16 (2022) 5874–5884, https://doi.org/10.1021/acsnano.1c11041.
[17] J. Jing, A. Herlopian, I. Karakis, M. Ng, J.J. Halford, A. Lam, D. Maus, F. Chan, M. Dolatshahi, C.F. Muniz, C. Chu, V. Sacca, J. Pathmanathan, W.D. Ge, H.Q. Sun, J. Dauwels, A.J. Cole, D.B. Hoch, S.S. Cash, M.B. Westover, JAMA Neurol. 77 (2020) 49–57, https://doi.org/10.1001/jamaneurol.2019.3531.
[18] J. Coult, J. Blackwood, L. Sherman, T.D. Rea, P.J. Kudenchuk, H. Kwok, Circ. Arrhythm. Electro 12 (2019) 1–10, https://doi.org/10.1161/CIRCEP.118.006924.
[19] S. Shen, X. Xiao, X. Xiao, J. Chen, A.C.S. Appl, Energy Mater. 5 (2022) 3952–3965, https://doi.org/10.1021/acsaem.1c02465.
[20] H. Yu, C. Wang, F.Y. Meng, D.Q. Zou, J.H. Li, Z.W. Song, M. Zhao, L. Zhang, S. S. Xu, L. Wang, IEEE Sens. J. 21 (2021) 25616–25623, https://doi.org/10.1109/JSEN.2021.3117994.
[21] J.X. Dai, H.R. Zhao, X.Z. Lin, S. Liu, Y.S. Liu, X.P. Liu, T. Fei, T. Zhang, ACS Appl. Mater. Interfaces 11 (2019) 6483–6490, https://doi.org/10.1021/acsami.8b18904.
[22] Z. Zhen, Z.C. Li, X.L. Zhao, Y.J. Zhong, L. Zhang, Q. Chen, T.T. Yang, H.W. Zhu, Small 14 (2018) 1703848, https://doi.org/10.1002/smll.201703848.
[23] Z. Nie, J.W. Kwak, M. Han, J.A. Rogers, Adv. Mater. (2022) 2205609, https://doi.org/10.1002/adma.202205609.
[24] Y. Wang, L. Qiu, Y.J. Luo, R. Ding, F. Jiang, Mech. Syst. Signal Process 141 (2020), 106730, https://doi.org/10.1016/j.ymssp.2020.106730.
[25] Y. Wang, L. Qiu, Y.J. Luo, R. Ding, Struct. Health Monit. 20 (2021) 861–876, https://doi.org/10.1177/1475921719850641.
[26] Y. Wang, S.G. Hu, T. Xiong, Y.A. Huang, L. Qiu, Struct. Health Monit. 21 (2022) 2453–2480, https://doi.org/10.1177/14759217211056831.
[27] R. Ghosh, M.S. Song, J. Park, Y. Tchoe, P. Guha, W. Lee, Y. Lim, B. Kim, S.W. Kim, M. Kim, G.C. Yi, Nano Energy 80 (2021), 105537, https://doi.org/10.1016/j.nanoen.2020.105537.
[28] G. Ge, Y.C. Cai, Q.C. Dong, Y.Z. Zhang, J.J. Shao, W. Huang, X.C. Dong, Nanoscale 10 (2018) 10033–10040, https://doi.org/10.1039/C8NR02813C.
[29] Y. Khan, A.E. Ostfeld, C.M. Lochner, A. Pierre, A.C. Arias, Adv. Mater. 28 (2016) 4373–4395, https://doi.org/10.1002/adma.201504366.

[30] R. Zhao, C. Yang, H.G. Wang, K. Jiang, H. Wu, S.P. Shen, L. Wang, Y. Sun, K.J. Jin, J. Gao, L. Chen, H.Y. Wang, J.L. MacManus-Driscoll, P.A. van Aken, J.W. Hong, W. W. Li, H. Yang, Nat. Commun. 13 (2022) 1–9, https://doi.org/10.1038/s41467-022-30074-4.
[31] W.W. Li, J.L. Shi, K.H.L. Zhang, J.L. MacManus-Driscoll, Mater. Horiz. 7 (2020) 2832–2859, https://doi.org/10.1039/D0MH00899K.
[32] W.W. Li, B.N. Zhu, R.X. Zhu, Q. Wang, P. Lu, Y.W. Sun, C. Cafolla, Z.M. Qi, A. P. Chen, P. Gao, H.Y. Wang, Q. He, K.H.L. Zhang, J.L. MacManus-Driscoll, Adv. Funct. Mater. 30 (2020) 2001984, https://doi.org/10.1002/adfm.202001984.
[33] X.Y. Zhang, Y. Wang, X.Y. Gao, Y.D. Ji, F.J. Qian, J.Y. Fan, H.Y. Wang, L. Qiu, W. W. Li, H. Yang, ACS Appl. Mater. Interfaces 13 (2021) 47764–47772, https://doi.org/10.1021/acsami.1c13704.
[34] R.X. Xu, L.L. Min, Z.M. Qi, X.Y. Zhang, J. Jian, Y.D. Ji, F.J. Qian, J.Y. Fan, C.X. Kan, H.Y. Wang, W. Tian, L. Li, W.W. Li, H. Yang, ACS Appl. Mater. Interfaces 12 (2020) 16462–16468, https://doi.org/10.1021/acsami.0c01298.
[35] M.B. Salamon, M. Jaime, Rev. Mod. Phys. 73 (2001) 583–628, https://doi.org/10.1103/RevModPhys.73.583.
[36] J.M. Rondinelli, N.A. Spaldin, Adv. Mater. 23 (2011) 3363–3381, https://doi.org/10.1002/adma.201101152.
[37] Y. Tokura, N. Nagaosa, Science 288 (2000) 462–468, https://doi.org/10.1126/science.288.5465.462.
[38] E. Dagotto, Science 309 (2005) 257–262, https://doi.org/10.1126/science.1107559.
[39] Y.J. Liu, S.J. Song, P. Gong, L.J. Xu, K.F. Li, D. Li, H.G. Wang, J.Y. Fan, L. Qiu, X. B. Tang, W.W. Li, H. Yang, Appl. Phys. Lett. 121 (2022), 122902, https://doi.org/10.1063/5.0101325.
[40] E.J. Guo, T. Charlton, H. Ambaye, R.D. Desautels, H.N. Leemd, M.R. Fitzsirnrnons, ACS Appl. Mater. Interfaces 9 (2017) 19307–19312, https://doi.org/10.1021/acsami.7b03252.
[41] S. Majumdar, S. van Dijken, J. Phys. D 47 (2014) 1–15, https://doi.org/10.1088/0022-3727/47/3/034010.
[42] F.J. Wang, C.G. Yang, Z.V. Vardeny, X.G. Li, Phys. Rev. B 75 (2007) 1–7, https://doi.org/10.1103/PhysRevB.75.245324.
[43] X.K. Ning, Z.J. Wang, Z.D. Zhang, Adv. Funct. Mater. 24 (2014) 5393–5401, https://doi.org/10.1002/adfm.201400735.
[44] X. Sun, Q. Li, J.J. Huang, M. Fan, B.X. Rutherford, R.L. Paldi, J. Jian, X.H. Zhang, H.Y. Wang, Appl. Mater. Today 16 (2019) 204–212, https://doi.org/10.1016/j.apmt.2019.05.012.
[45] A.P. Chen, Z.X. Bi, C.F. Tsai, J. Lee, Q. Su, X.H. Zhang, Q.X. Jia, J.L. MacManus-Driscoll, H.Y. Wang, Adv. Funct. Mater. 21 (2011) 2423–2429, https://doi.org/10.1002/adfm.201002746.
[46] D. Le Bourdais, G. Agnus, T. Maroutian, V. Pillard, P. Aubert, R. Bachelet, G. Saint-Girons, B. Vilquin, E. Lefeuvre, P. Lecoeur, J. Appl. Phys. 118 (2015), 124509, https://doi.org/10.1063/1.4931885.
[47] O. Al-Dossary, A. Umar, A.A. Al-Harbi, S.A. Zaidi, G.N. Dar, J. Nanosci. Nanotechnol. 12 (2012) 6368–6373, https://doi.org/10.1166/jnn.2012.6445.
[48] Z.H. Duan, M. Xu, T.S. Li, Y. Zhang, H.F. Zou, Sens. Actuators B Chem. 258 (2018) 527–534, https://doi.org/10.1016/j.snb.2017.11.169.
[49] M. Guo, C. Yang, D. Gao, Q. Li, A.H. Zhang, J.J. Feng, H. Yang, R.Q. Tao, Z. Fan, M. Zeng, G.F. Zhou, X.B. Lu, J.M. Liu, J. Mater. Sci. Technol. 44 (2020) 42–47, https://doi.org/10.1016/j.jmst.2019.10.019.
[50] G. Kandasamy, Nanotechnology 30 (2019) 1–32, https://doi.org/10.1088/1361-6528/ab3f17.
[51] L.X. Ye, D. Zhang, J.J. Lu, S.C. Xu, R.X. Xu, J.Y. Fan, R.J. Tang, H.Y. Wang, H. Z. Guo, W.W. Li, H. Yang, J. Phys. D 55 (2022), 224002, https://doi.org/10.1088/1361-6463/ac570d.
[52] Y.T. Zhang, Y.Q. Cao, H. Hu, X. Wang, P.Z. Li, Y. Yang, J. Zheng, C. Zhang, Z. Q. Song, A.D. Li, Z. Wen, ACS Appl. Mater. Interfaces 11 (2019) 8284–8290, https://doi.org/10.1021/acsami.8b22664.
[53] G. Li, D.G. Xie, Z.Y. Zhang, Q.L. Zhou, H. Zhong, H. Ni, J.O. Wang, E.J. Guo, M. He, C. Wang, G.Z. Yang, K.J. Jin, C. Ge, Adv. Funct. Mater. 32 (2022) 2203074, https://doi.org/10.1002/adfm.202203074.
[54] A. Tricoli, N. Nasiri, S.Y. De, Adv. Funct. Mater. 27 (2017) 1605271, https://doi.org/10.1002/adfm.201605271.
[55] J.X. Dai, X. Guan, H.R. Zhao, S. Liu, T. Fei, T. Zhang, Sens. Actuators B Chem. 316 (2020), 128159, https://doi.org/10.1016/j.snb.2020.128159.
[56] K. Wu, X. Guan, Z.N. Hou, L.C. Liu, H.R. Zhao, S. Liu, T. Fei, T. Zhang, J. Colloid Interface Sci. 602 (2021) 646–653, https://doi.org/10.1016/j.jcis.2021.06.064.
[57] R.A. Shaukat, M.U. Khan, Q.M. Saqib, M.Y. Chougale, J. Kim, J. Bae, Sens. Actuators B Chem. 345 (2021), 130371, https://doi.org/10.1016/j.snb.2021.130371.
[58] P. Barthel, R. Wensel, A. Bauer, A. Muller, P. Wolf, K. Ulm, K.M. Huster, D. P. Francis, M. Malik, G. Schmidt, Eur. Heart J. 34 (2013) 1644–1650, https://doi.org/10.1093/eurheartj/ehs420.
[59] M.J. Tipton, A. Harper, J.F.R. Paton, J.T. Costello, J. Physiol. 595 (2017) 5729–5752, https://doi.org/10.1113/JP274596.
[60] A. Nicolo, S.M. Marcora, I. Bazzucchi, M. Sacchetti, Exp. Physiol. 102 (2017) 934–949, https://doi.org/10.1113/EP086352.
[61] D.P. Tashkin, M.D. Altose, J.E. Connett, R.E. Kanner, W.W. Lee, R.A. Wise, Am. J. Respir. Crit. Care Med. 153 (1996) 1802–1811, https://doi.org/10.1164/ajrccm.153.6.8665038.
[62] A. Kumar, A. Kosonowski, P. Wyzga, K.T. Wojciechowski, J. Eur. Ceram. Soc. 41 (2021) 451–458, https://doi.org/10.1016/j.jeurceramsoc.2020.08.069.
[63] Y. Feng, Z.Y. He, Z.J. Yang, W.X. Tang, Q.G. Chi, Q.G. Chen, J. Appl. Polym. Sci. 139 (2022), e53034, https://doi.org/10.1002/app.53034.
[64] E.W. Lemmon, R.T. Jacobsen, Int J. Thermophys. 25 (2004) 21–69, https://doi.org/10.1023/B:IJOT.0000022327.04529.f3.
[65] J.Y. Fan, L.S. Xu, X.Y. Zhang, Y.G. Shi, W.C. Zhang, Y. Zhu, B.T. Gao, B. Hong, L. Zhang, W. Tong, L. Pi, Y.H. Zhang, J. Mater. Sci. 50 (2015) 2130–2137, https://doi.org/10.1007/s10853-014-8775-1.
[66] A. Ueno, J. Kim, H. Nagano, Int. J. Heat. Mass Transf. 166 (2021), 120631, https://doi.org/10.1016/j.ijheatmasstransfer.2020.120631.

Lianxu Ye is a fourth year Ph.D. candidate in the College of Physics at Nanjing University of Aeronautics and Astronautics advised by Prof. Hao Yang. He graduated from Nanjing University of Aeronautics and Astronautics with a Bachelor's degree in Applied Physics. His research interest is developing flexible perovskite oxide thin film and exploring their potential applications in multifunctional sensors.

Fan Wu received her Bachelor's degree in 2020, and Master's degree from Nanjing University of Aeronautics and Astronautics in 2023 advised by Prof. Guili Xu. Her research interest is computer vision and software development.

Dr. Ruixing Xu received his Bachelor's degree from Nanjing University of Technology in 2012 and his Ph.D. degree from Nanjing University of Aeronautics and Astronautics in 2022 advised by Prof. Hao Yang. At present, he works in School of Microelectronics & Data Science at Anhui University of Technology. His mainly research interests include strongly correlated electron systems, transparent conductive oxide films.

Dr. Di Zhang received his Bachelor's degree from Northwestern Polytechnical University and Master's degree from Shanghai Jiao Tong University in China. He received his Ph.D. degree from School of Materials Engineering at Purdue University in May 2021. He is currently a Director's Postdoc Fellow working at Center for Integrated Nanotechnologies (CINT) at Los Alamos National Laboratory. His research interests include developing self-assembled nanocomposite functional thin films towards nanoelectronic and nanophotonic device applications, and utilizing advanced electron microscopy techniques to study complex functional oxides and electronic devices.

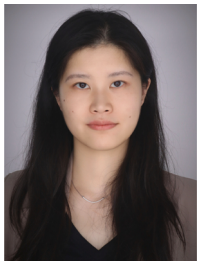

Juanjuan Lu is a fourth year Ph.D. student in the department of Materials Engineering at Purdue University, under the supervision of Prof. Haiyan Wang. She received her Bachelor's degree from Central South University in 2016 and Master's from Zhejiang University in 2019. Her current research is focused on the microstructural design of self-assembled vertically aligned oxide-metal nanocomposite systems, and the multifunctionality coupling relationships, including mainly optical and ferromagnetic properties.

Chuanlong Wang received his Bachelor's degree from Anhui Normal University in 2020 and began to pursue a Master's degree in the School of Physical Science and Technology of Soochow University in 2020. He joined Prof. Rujun Tang's team in 2020. At present, the research content is mainly flexible ferroelectric materials.

Anjiang Dong received his Bachelor's degree from WEZHENG COLLEGE of SOOCHOW UNIVERSITY in 2020 and his Master's degree from School of Physical Science and Technology of Soochow University in 2020. He joined Prof. Rujun Tang's team in 2020. At present, the research content is mainly magnetoelectric materials and devices.

Sichen Xu graduated with a Bachelor's degree in physics from Soochow University and obtained a Master's degree from the School of Physical Science and Technology, Soochow University in 2021. He has published one paper in Scripta Materials and has been granted one national invention patent.

Lejun Xue received his Bachelor's degree from Anhui University in 2021 and began to pursue a Master's degree in the School of Physical Science and Technology of Soochow University in 2021. He joined Prof. Rujun Tang's team in 2021. At present, the research content is mainly magnetic materials and devices.

Zixin Fan received his Bachelor's degree from Suzhou City University in 2016 and his Master's degree under the supervision of Prof. Run Zhao at Suzhou University of Science and Technology in 2023. His current research interest mainly focuses on the Magnetic two-dimensional electron gas at oxide interface.

Longjie Xu is currently a first-year doctoral student at the College of Physics, Nanjing University of Aeronautics and Astronautics, under the supervision of Prof. Hao Yang. His main research interest is piezoelectric materials for structural health monitoring of aircraft, with a view to their potential engineering applications.

Kaifeng Li is currently a Ph.D. candidate in the College of Physics, Nanjing University of Aeronautics and Astronautics under the direction of Prof. Hao Yang and Prof. Weiwei Li. His research focuses on the development of functional oxide films including memristors, transparent conducting oxides, and their applications.

Dong Li currently is a Ph.D. candidate working in Prof. Weiwei Li's group in MIIT Key Laboratory of Aerospace Information Materials and Physics, College of Physics, Nanjing University of Aeronautics and Astronautics, mainly focusing on the new physical properties of oxide films and interfaces and their regulation.

Dr. Ahmed Kursumovic is a senior research associate in Prof. Judith MacManus-Driscoll's group in the Department of Materials Science & Metallurgy at the University of Cambridge. His research focuses on energy materials, notably superconductors and charge storage materials.

Dr. Run Zhao received his Ph.D. from Soochow University in 2014. He joined Suzhou university of science and technology in 2015. His research interests include multiferroic thin film, vertical interface, and two-dimensional electron gas.

Professor Rujun Tang is a professor of School of Physical Science and Technology, Soochow University. Professor Tang's expertise focuses on the understanding of multi-dimensional physical properties of integrated magnetoelectric materials, and developing high-performance magnetic and electrical functional materials and devices. He has published more than 70 research papers in professional journals and was granted 7 national invention patents. He is the senior member of the applied magnetism branch of the Chinese Electronics Society.

Professor Lei Qiu is a professor of college of Aerospace Engineering, Nanjing University of Aeronautics and Astronautics. Professor Qiu's expertise focuses on aircraft intelligent structure and health monitoring. He has published more than 140 research papers in professional journals and was granted 60 Chinese and US invention patents and won the China Youth Science and Technology Award in 2022. He is a member of the Youth Work Committee of the Chinese Aviation Society.

Professor Haiyan Wang is the Basil S. Turner Professor of Engineering with a joint appointment between the Schools of Materials Engineering and Electrical and Computer Engineering. Professor Wang's expertise is in electronic ceramic materials and covers processing and characterization of oxide- and nitride-based thin films in nanocomposite form for microelectronics, photonics, optoelectronics, ferroelectric and multiferroics, superconductors, solid oxide fuel cells, and batteries. She has published more than 490 journal papers (total citation over 16500, H-Factor 62), and is a Fellow of ASM International, ACerS, AAAS, APS and MRS.

Prof. Judith MacManus-Driscoll is a Professor in the Materials Science & Metallurgy at the University of Cambridge. She is also Royal Academy of Engineering Chair in Emerging Technologies. Her research work is in the area of oxide thin film engineering for low power electronic and energy devices. She is interested both in understanding basic functionalities and in engineering new interfacial-driven properties.

Dr. Qingshen Jing is a lecturer in the James Watt School of Engineering at the University of Glasgow, UK. He received his joint Ph.D. degree from Peking University (China) and Georgia Institute of Technology (USA) in 2015. He was a Marie Curie research fellow and a research associate in the Department of Materials Science & Metallurgy at the University of Cambridge (UK) from 2016 to 2022. His research interests lie in wearable and implantable electronics and energy harvesting devices using advanced fabrication technology including additive manufacturing.

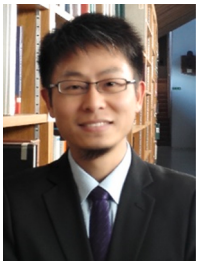

Prof. Weiwei Li is a Professor in the College of Physics at the Nanjing University of Aeronautics and Astronautics. His research interests focus on the complex functional oxide thin films for low-energy consumption (opto-)electronic devices and energy conversion/storage. He obtained his Ph.D. degree from Soochow University in 2015, followed by working as a research associate in the Department of Materials Science & Metallurgy at the University of Cambridge from 2015 to 2021.

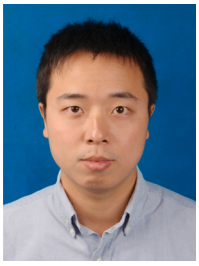

Professor Hao Yang received his Ph.D. degree from Institute of Physics, Chinese Academy of Sciences in 2005. Currently, he is a Professor in the College of Physics at Nanjing University of Aeronautics and Astronautics. He is mainly engaged in the research of artificially structured oxide thin films and ferroelectric and multiferroic thin films, which provide ideas for solving the key problems of the application of thin films in the field of aerospace, and has published more than 120 SCI papers in *Advanced Materials*, *Nature Materials*, *PRL* and other well-known international journals.